

Bounds on the electromagnetic dipole moments through the single top production at the CLIC

M. Köksal*,¹ A. A. Billur†,² and A. Gutiérrez-Rodríguez‡³

¹*Department of Optical Engineering, Cumhuriyet University, 58140, Sivas, Turkey.*

²*Department of Physics, Cumhuriyet University, 58140, Sivas, Turkey.*

³*Facultad de Física, Universidad Autónoma de Zacatecas*

Apartado Postal C-580, 98060 Zacatecas, México.

(Dated: November 19, 2021)

Abstract

We obtain bounds on the anomalous magnetic and electric dipole moments of the t -quark from a future high-energy and high-luminosity linear electron-positron collider, as the CLIC, with polarized and unpolarized electron beams which are powerful tools for determining new physics. We consider the processes $\gamma e^- \rightarrow \bar{t} b \nu_e$ (γ is the Compton backscattering photon) and $e^+ e^- \rightarrow e^- \gamma^* e^+ \rightarrow \bar{t} b \nu_e e^+$ (γ^* is the Weizsacker-Williams photon) as they are one of the most important sources of single top-quark production. For systematic uncertainties of $\delta_{sys} = 0\%$ (5%), b -tagging efficiency = 0.8, center-of-mass energy of $\sqrt{s} = 3 \text{ TeV}$ and integrated luminosity of $\mathcal{L} = 2 \text{ ab}^{-1}$ the future $e^+ e^-$ collider may put bounds on the electromagnetic dipole moments \hat{a}_V and \hat{a}_A of the top quark of the order of $\mathcal{O}(10^{-2} - 10^{-1})$ at the 2σ (3σ) level, which are competitive with those recently reported in previous studies at hadron colliders and the ILC.

PACS numbers: 14.65.Ha, 13.40.Em

Keywords: Top quarks, Electric and Magnetic Moments.

* mkoksal@cumhuriyet.edu.tr

† abillur@cumhuriyet.edu.tr

‡ alexgu@fisica.uaz.edu.mx

I. INTRODUCTION

The top quark is by far the heaviest particle of the Standard Model (SM) [1–3], with a mass of $m_t = 173.5 \pm 0.6$ (stat.) ± 0.8 (syst.) [4]. Up to now, the top quark has only been studied at the Tevatron and Large Hadron Collider (LHC). Its large mass implies that the top quark is the SM particle most strongly coupled to the mechanism of electroweak symmetry breaking. This is the principal reason it is considered to be one of the most likely places where new physics might be discovered. This means the top quark is a window to any new physics at the TeV energy scale. While much information about the top quark is already available that shows consistency with SM expectations, its properties and interactions are among the most important measurements for present and future high energy colliders [5–13].

The construction of a high-energy e^+e^- International Linear Collider (ILC) has been proposed to complement direct searches carried out at the LHC. Precision measurements of top quark properties, in particular of its couplings, are especially interesting because the top quark is the heaviest known elementary particle and thus expected to be more sensitive to new physics at higher scales.

The top quark has been studied in some detail at the Tevatron and LHC. Many of its properties are still poorly constrained such as mass, spin, color and electric charges, the electric and magnetic dipole moments and the chromomagnetic and chromoelectric dipole moments. Therefore, significant new insights on top quark properties will be one of the tasks of the LHC, the ILC [7–9] and the Compact Linear Collider (CLIC) [11, 14].

The dipole moments of the top quark are some of the most sensitive observable, and although these intrinsic properties have been studied extensively both theoretically and experimentally, it is necessary to have more precise measurements. The dipole moments of the top quark have been investigated by several authors and in a variety of theoretical models [15–22]. Further, a number of studies show that in the processes $e^+e^- \rightarrow t\bar{t}$ and $\gamma\gamma \rightarrow t\bar{t}$, the dipole moments of the top quark can be measured with great sensitivity [23–26]. However, there are a significant number of top quarks that are produced in single form via the weak interaction. There are several single top quark production processes of interest in e^+e^- , e^-e^- , γe^- and $\gamma\gamma$ collisions, characterized by the virtuality of the W boson [27–36].

Although studying single top quark production may not be considered of great importance, there are several reasons why its study is necessary in future linear e^+e^- colliders:

1) It is a very good alternative to study the dipole moments \hat{a}_V and \hat{a}_A of the top quark, as well as the anomalous coupling tbW . 2) Single top production at CLIC in association with a W boson and bottom quark through WW^* production leads to the same final state as t quark pair production. 3) The cross section for single top quark production processes is significant since production is abundant in e^+e^- colliders that operate at high energies. In addition, the single top quark production is directly proportional to the square of the tbW coupling, and therefore it is potentially very sensitive to the tbW structure [37]. 4) Single top quarks are produced with nearly 100% polarization due to the weak interaction [38, 39]. 5) New physics can influence single top production by inducing weak interactions beyond the SM weak interactions [39, 40], through loop effects [41–43], or by providing new sources of single top quark production [44–46]. For these reasons, it is important to study the properties of the top quark, in particular their dipole moments through the single top quark production processes.

In the SM, the prediction for the Magnetic Dipole Moment (MDM) of the top quark is $a_t^{SM} = 0.02$ [47], which can be tested in current and future colliders, such as LHC and CLIC. In contrast, its Electric Dipole Moment (EDM) is strongly suppressed and less than 10^{-30} ecm [15, 48, 49], which is much too small to be observed. It is, however, highly attractive for probing new physics.

The sensitivity to the EDM has been studied in models with vector-like multiplets which predicted the top quark EDM close to 1.75×10^{-3} [50].

There are studies performed via the $t\bar{t}\gamma$ production for the LHC at $\sqrt{s} = 14 TeV$ and $\mathcal{L} = 300 fb^{-1}$ and $3000 fb^{-1}$, with limits of ± 0.2 and ± 0.1 , respectively [51]. Other limits are reported in the literature: $-2.0 \leq \hat{a}_V \leq 0.3$ and $-0.5 \leq \hat{a}_A \leq 1.5$ which are obtained from the branching ratio and the CP asymmetry from radiative $b \rightarrow s\gamma$ transitions [52], while the bounds of $|\hat{a}_V| < 0.05$ (0.09) and $|\hat{a}_A| < 0.20$ (0.28) come from measurements of $\gamma p \rightarrow t\bar{t}$ cross section with 10% (18%) uncertainty, respectively [53]. More recent limits on the top quark magnetic and electric dipole moments through the process $pp \rightarrow p\gamma^*\gamma^*p \rightarrow pt\bar{t}p$ at the LHC with $\sqrt{s} = 14 TeV$, $\mathcal{L} = 3000 fb^{-1}$ and 68% C.L. are $-0.6389 \leq \hat{a}_V \leq 0.0233$ and $|\hat{a}_A| \leq 0.1158$ [54]. Sensitivity limits for the anomalous couplings of the top quark through the production process of top quark pairs $e^+e^- \rightarrow t\bar{t}$ for the ILC at $\sqrt{s} = 500 GeV$, $\mathcal{L} = 200 fb^{-1}$, $\mathcal{L} = 300 fb^{-1}$ and $\mathcal{L} = 500 fb^{-1}$ are predicted to be of the order of $\mathcal{O}(10^{-3})$. Thus, the measurements at an electron positron collider lead to a significant improvement in

comparison with LHC. Detailed discussions on the dipole moments of the top quark in top quark pairs production at the ILC are reported in the literature [7–10, 13, 23–26, 55–57]. It is worth mentioning that there are no limits reported in the literature on the dipole moments \hat{a}_V and \hat{a}_A via single top quark production processes.

CP violation was first observed in a small fraction of K mesons decaying to two pions in the SM. This phenomenology in the SM can be easily introduced by the Cabibbo-Kobayashi-Maskawa mechanism in the quark sector. For this reason, the presence of new physics beyond the SM can be investigated by examining the electromagnetic properties of the top quark that are defined with CP-symmetric and CP-asymmetric anomalous form factors. Its dipole moments such as the MDM come from one-loop level perturbations and the corresponding EDM, which is described as a source of CP violation.

Following references [51, 54, 58–60], the definition of the general effective coupling $t\bar{t}\gamma$, including the SM coupling and contributions from dimension-six effective operators, can be parameterized by the following effective Lagrangian:

$$\mathcal{L}_{\gamma t\bar{t}} = -g_e Q_t \bar{t} \Gamma_{\gamma t\bar{t}}^\mu t A_\mu, \quad (1)$$

where g_e is the electromagnetic coupling constant, Q_t is the top quark electric charge and $\Gamma_{\gamma t\bar{t}}^\mu$ the Lorentz-invariant vertex function which describes the interaction of a γ photon with two top quarks and can be parameterized by

$$\Gamma_{\gamma t\bar{t}}^\mu = \gamma^\mu + \frac{i}{2m_t} (\hat{a}_V + i\hat{a}_A \gamma_5) \sigma^{\mu\nu} q_\nu, \quad (2)$$

where m_t is the mass of the top quark, q is the momentum transfer to the photon and the couplings \hat{a}_V and \hat{a}_A are real and related to the anomalous magnetic moment and the electric dipole moment of the top quark, respectively.

The majority of physics research in linear colliders is done assuming positron and electron beams are unpolarized. However, another significant advantage of the linear colliders is to obtain suitability of a highly polarized electron beam that can be polarized up to $\pm 80\%$. A polarized electron beam provides a method to investigate the SM and to diagnose new physics beyond the SM. Observation of even the tiniest signal which conflicts with the SM expectations would be persuasive evidence for new physics. Proper selection of the electron beam polarization may therefore be used to enhance the new physics signal and also to

considerably suppress backgrounds.

In this work we study the sensibility of the anomalous magnetic and electric dipole moments of the top quark through the processes $\gamma e^- \rightarrow \bar{t} b \nu_e$ (γ is the Compton backscattering photon) and $e^+ e^- \rightarrow e^- \gamma^* e^+ \rightarrow \bar{t} b \nu_e e^+$ (γ^* is the Weizsacker-Williams photon) which are among the most important sources of single top quark production [27, 30]. We use center-of-mass energies of the CLIC [14]. These values are for a center-of-mass energy of 1.4 TeV with integrated luminosity of 1500 fb^{-1} and 3 TeV with $\mathcal{L} = 2000 \text{ fb}^{-1}$, and polarized and unpolarized electron beams $P_{e^-} = -80\%$ and $P_{e^+} = 0\%$ [61]. Not only can the future $e^+ e^-$ linear collider be designed to operate in $e^+ e^-$ collision mode, but it can also be operated as a $e\gamma$ and $\gamma\gamma$ collider. This is achieved by using Compton backscattered photons in the scattering of intense laser photons on the initial $e^+ e^-$ beams. Another well-known application of linear colliders is to study new physics beyond the SM through $e\gamma^*$ and $\gamma^*\gamma^*$ collisions. A quasireal γ^* photon emitted from one of the incoming e^- or e^+ beams interacts with the other lepton shortly after, generating the subprocess $\gamma^* e^- \rightarrow \bar{t} b \nu_e$. Hence, first we calculate the main reaction $e^+ e^- \rightarrow e^- \gamma^* e^+ \rightarrow \bar{t} b \nu_e e^+$ by integrating the cross section for the subprocess $\gamma^* e^- \rightarrow \bar{t} b \nu_e$. In this case, the quasireal photons in $\gamma^* e^-$ collisions can be examined by Equivalent Photon Approximation (EPA) [62–64] using the Weizsacker-Williams approximation (WWA). In EPA, photons emitted from incoming leptons which have very low virtuality are scattered at very small angles from the beam pipe. These emitted quasireal photons have a low Q^2 virtuality and are therefore almost real. We only use the photon virtuality of $Q_{max}^2 = 2 \text{ GeV}^2$. Also, we can add parts related to the large values of Q_{max}^2 which do not significantly contribute to obtaining sensitivity limits on the anomalous couplings [65–68]. These processes have been observed phenomenologically and experimentally at the LEP, Tevatron and LHC [69–90].

Taking all of the aforementioned into account, we study the potential of the processes $\gamma e^- \rightarrow \bar{t} b \nu_e$ and $e^+ e^- \rightarrow e^+ \gamma^* e^- \rightarrow \bar{t} b \nu_e e^+$ via Compton backscattering and WWA, respectively, and derive bounds on the dipole moments \hat{a}_V and \hat{a}_A at 2σ and 3σ level (90% and 95% C.L.), and at a future high-energy and high-luminosity linear electron positron collider, as the CLIC, to study the sensibility on the anomalous magnetic and electric dipole moments of the top quark. The corresponding schematic and Feynman diagrams for the main reactions as well as for the subprocesses which give the most significant contribution to the total cross section are shown in Figs. 1-2.

This paper is organized as follows. In Section II, we study the dipole moments of the top quark through the process $\gamma e^- \rightarrow \bar{t} b \nu_e$ and in Section III, through the process $e^+ e^- \rightarrow e^+ \gamma^* e^- \rightarrow \bar{t} b \nu_e e^+$. Finally, we summarize our conclusions in Section IV.

II. COMPTON BACKSCATTERING: CROSS SECTION OF $\gamma e^- \rightarrow \bar{t} b \nu_e$

In this section we present numerical results of the cross section for the process $\gamma e^- \rightarrow \bar{t} b \nu_e$, using the CalcHEP [91] packages for calculations of the matrix elements and cross sections. These packages provide automatic computation of the cross sections and distributions in the SM as well as their extensions at tree level. We consider the high-energy stage of possible future linear γe^- collisions with $\sqrt{s} = 1.4$ and $3 TeV$ and design luminosity 50, 300, 500, 1000, 1500 and 2000 fb^{-1} according to the new data reported by the CLIC [14]. In addition, in all numerical analysis we consider the b -tagging efficiency of 0.8, systematic uncertainty of $\delta_{sys} = 0\%, 5\%$ and the acceptance cuts will be imposed as $|\eta^b| < 2.5$ for pseudorapidity, $p_T^b > 20 GeV$ and $p_T^{\nu_e} > 10 GeV$ for transverse momenta of the final state particles. We also consider the hadronic decay channels of the top quark $BR = 0.676$ (Hadronic branching ratio). There are systematic uncertainties for hadron colliders for single top quark production [92]. For example, these uncertainties arise from luminosity, jet identification, backgrounds, b -tagging efficiency, etc.. On the other hand, linear colliders have less uncertainties with respect to hadron colliders for determination of the cross section of single top quark production [93]. Therefore, for events estimation in χ^2 analysis, we have taken into account b -tagging efficiency as well as consider systematic uncertainties of 0% and 5%. The values close to this systematic uncertainty value have been taken into account in previous studies, for example in Ref. [94], a 3% systematic error in the total cross section has been assumed for the $e^- e^+ \rightarrow t \bar{t}$ process at the ILC. It can be seen that the systematic error in the cross section determination has been lowered from 3% to 1% [95]. However, since there is no study related to the systematic error on the single top quark production at the CLIC, we use systematic errors of 0% and 5% for the processes studied in this paper.

In our study we examined the projected 2σ and 3σ sensitivities on the dipole moments \hat{a}_V and \hat{a}_A of the top quark for the processes $\gamma e^- \rightarrow \bar{t} b \nu_e$ (γ is the Compton backscattering photon) and $e^+ e^- \rightarrow e^- \gamma^* e^+ \rightarrow \bar{t} b \nu_e e^+$ (γ^* is the Weizsacker-Williams photon) at the CLIC-1.4 TeV and CLIC-3 TeV , respectively. We use the chi-squared distribution test defined

as

$$\chi^2 = \left(\frac{\sigma_{SM} - \sigma_{NP}(\hat{a}_V, \hat{a}_A)}{\sigma_{SM}\delta} \right)^2, \quad (3)$$

where $\sigma_{NP}(\hat{a}_V, \hat{a}_A)$ is the total cross section including contributions from the SM and new physics, $\delta = \sqrt{(\delta_{st})^2 + (\delta_{sys})^2}$, $\delta_{st} = \frac{1}{\sqrt{N_{SM}}}$ is the statistical error, δ_{sys} is the systematic error and N_{SM} is the number of signal expected events $N_{SM} = \mathcal{L}_{int} \times BR \times \sigma_{SM} \times \epsilon_b$ where $\epsilon_b = 0.8$ is the b -tagging efficiency and \mathcal{L}_{int} is the integrated CLIC luminosity.

A. Top quark dipole moments through the process $\gamma e^- \rightarrow \bar{t} b \nu_e$ with polarized and unpolarized beams

With polarized beams of electrons and positrons, the cross section of a process can be expressed as [61]

$$\begin{aligned} \sigma(P_{e^-}, P_{e^+}) = & \frac{1}{4} [(1 + P_{e^-})(1 + P_{e^+})\sigma_{++} + (1 - P_{e^-})(1 - P_{e^+})\sigma_{--} \\ & + (1 + P_{e^-})(1 - P_{e^+})\sigma_{+-} + (1 - P_{e^-})(1 + P_{e^+})\sigma_{-+}], \end{aligned} \quad (4)$$

where P_{e^-} (P_{e^+}) is the polarization degree of the electron (positron) beam, while σ_{-+} stands for the cross section for completely left-handed polarized e^- beam $P_{e^-} = -1$ and completely right-handed polarized e^+ beam $P_{e^+} = 1$, and other cross sections σ_{--} , σ_{++} and σ_{+-} are defined analogously.

The corresponding Feynman diagrams for the process $\gamma e^- \rightarrow \bar{t} b \nu_e$ that give the most important contribution to the total cross sections are shown in Fig. 2. In this figure the Feynman diagrams (1)-(3) correspond to the contribution of the SM, while diagram (4) corresponds to the anomalous contribution, i.e., for the γe^- collisions there is SM background at the tree level so the total cross section is proportional to $\sigma_{Tot} = \sigma_{SM} + \sigma_{Int}(\hat{a}_V, \hat{a}_A) + \sigma_{Anom}(\hat{a}_V^2, \hat{a}_A^2, \hat{a}_V \hat{a}_A)$, respectively.

To illustrate our results, we show the dependence of the cross section on the anomalous couplings \hat{a}_V and \hat{a}_A for $\gamma e^- \rightarrow \bar{t} b \nu_e$ in Fig. 3 for $P_{e^-} = -80\%$, $P_{e^+} = 0\%$, as well as on unpolarized beams and two different center-of-mass energies $\sqrt{s} = 1.4, 3 \text{ TeV}$ [14], whereas the \hat{a}_V (\hat{a}_A) anomalous coupling is kept fixed at zero. We observed that the cross section is sensitive to the value of the center-of-mass energies. The sensitivity to $\bar{t} b \nu_e$ increases with the

collider energy reaching a maximum at the end of the range considered, $\hat{a}_{V,A} = \pm 1$, and the cross section for $\sqrt{s} = 3 \text{ TeV}$ increases relative to $\sqrt{s} = 1.4 \text{ TeV}$ up to 24.5% with polarized beams and up to 26.6% with unpolarized beams. By contrast, in the vicinity of $\hat{a}_{V,A} = 0$ the total cross section is smaller. We notice that, as shown in Fig. 3, the $\gamma e^- \rightarrow \bar{t} b \nu_e$ production process at an CLIC-based γe^- collider reaches a value of $\sigma = 0.55 \text{ pb}$ (0.3 pb) for $\sqrt{s} = 3 \text{ TeV}$ for polarized and unpolarized beams. Although the cross section for unpolarized beams is approximately half of that of polarized beams, in both cases the $t\bar{t}\gamma$ coupling could be probed with remarkable sensitivity (see Tables I, II).

In Fig. 4 we used two center-of-mass energies $\sqrt{s} = 1.4, 3 \text{ TeV}$ expected for the CLIC accelerator in order to get contour limits in the plane $\hat{a}_V - \hat{a}_A$ for $\gamma e^- \rightarrow \bar{t} b \nu_e$ and the expected luminosities of $\mathcal{L} = 50, 500, 1500, 2000 \text{ fb}^{-1}$ with polarized and unpolarized beams of electrons and positrons.

As an indicator of the order of magnitude, using b -tagging efficiency of 0.8 and considering the systematic errors of $\delta_{sys} = 0\%, 5\%$, in Tables I and II we present the bounds obtained on the \hat{a}_V magnetic moment and \hat{a}_A electric dipole moments of the t -quark with the polarization $P_{e^-} = -80\%$ for the electron beams, $P_{e^+} = 0\%$ for the positron, as well as with unpolarized beams, with $\sqrt{s} = 1.4, 3 \text{ TeV}$, $\mathcal{L} = 50, 300, 500, 1000, 1500, 2000 \text{ fb}^{-1}$ at 2σ and $3\sigma \text{ C.L.}$, respectively. As expected, the results presented in Tables I and II clearly show that as the energy and luminosity of the collider increase, the bounds on the dipole moments of the top quark are stronger. We observed that these results are competitive with those recently reported in previous studies [51–54]. From results presented in Table I, it is obvious that the effect of polarized beams is more significant than the effect of unpolarized beams (see Table II).

To complement our results, in Table III we show the single top production total cross section for the process $\gamma e^- \rightarrow \bar{t} b \nu_e$ as a function of the dipole moments \hat{a}_V and \hat{a}_A at the two CLIC energies of 1.4 and 3 TeV. For polarized beams ($P_{e^-,e^+} = -80\%, 0\%$), the total cross section most significant for the process considered is $\sigma_{Tot}(\gamma e^- \rightarrow \bar{t} b \nu_e) = 5.4330 \times 10^{-1} \text{ pb}$ for $\hat{a}_V = -1$, $\hat{a}_A = 0$ and $\sqrt{s} = 3 \text{ TeV}$, while for $\hat{a}_A = 1$, $\hat{a}_V = 0$ and $\sqrt{s} = 3 \text{ TeV}$ the total cross section is $\sigma_{Tot}(\gamma e^- \rightarrow \bar{t} b \nu_e) = 5.3923 \times 10^{-1} \text{ pb}$. On the other hand, for unpolarized beams ($P_{e^-,e^+} = 0\%, 0\%$), the total cross sections are $\sigma_{Tot}(\gamma e^- \rightarrow \bar{t} b \nu_e) = 3.0186 \times 10^{-1} \text{ pb}$ for $\hat{a}_V = -1$, $\hat{a}_A = 0$ and $\sigma_{Tot}(\gamma e^- \rightarrow \bar{t} b \nu_e) = 2.9953 \times 10^{-1} \text{ pb}$ for $\hat{a}_V = 0$, $\hat{a}_A = -1$ with $\sqrt{s} = 3 \text{ TeV}$, respectively. Therefore, the total cross section for the case of polarized beams

TABLE I: Bounds on the \hat{a}_V magnetic moment and \hat{a}_A electric dipole moment for the process $\gamma e^- \rightarrow \bar{t}b\nu_e$ (γ is the Compton backscattering photon) for $P_{e^-,e^+} = -80\%, 0\%$, b -tagging efficiency = 0.8, $\delta_{sys} = 0\%, 5\%$ at 2σ and 3σ C.L.

2 σ C.L.		$\delta_{sys} = 0\%$		$\delta_{sys} = 5\%$	
\sqrt{s} (TeV)	\mathcal{L} (fb^{-1})	\hat{a}_V	$ \hat{a}_A $	\hat{a}_V	$ \hat{a}_A $
1.4	50	[-0.1091, 0.1565]	0.1615	[-0.1902, 0.2406]	0.2352
1.4	300	[-0.0630, 0.1103]	0.1032	[-0.1785, 0.2289]	0.2235
1.4	500	[-0.0534, 0.1007]	0.0908	[-0.1775, 0.2279]	0.2224
1.4	1000	[-0.0424, 0.0897]	0.0763	[-0.1767, 0.2271]	0.2217
1.4	1500	[-0.0369, 0.0842]	0.0689	[-0.1765, 0.2268]	0.2214
3	50	[-0.0724, 0.0816]	0.0768	[-0.1163, 0.1254]	0.1208
3	300	[-0.0447, 0.0539]	0.0491	[-0.1120, 0.1211]	0.1164
3	500	[-0.0389, 0.0480]	0.0432	[-0.1116, 0.1207]	0.1161
3	1000	[-0.0320, 0.0412]	0.0364	[-0.1113, 0.1204]	0.1158
3	1500	[-0.0286, 0.0377]	0.0329	[-0.1113, 0.1203]	0.1157
3	2000	[-0.0234, 0.0325]	0.0277	[-0.1112, 0.1203]	0.1156
3 σ C.L.		$\delta_{sys} = 0\%$		$\delta_{sys} = 5\%$	
1.4	50	[-0.1209, 0.1683]	0.1762	[-0.2096, 0.2599]	0.2567
1.4	300	[-0.0703, 0.1177]	0.1126	[-0.1968, 0.2472]	0.2438
1.4	500	[-0.0598, 0.1071]	0.0990	[-0.1957, 0.2460]	0.2427
1.4	1000	[-0.0477, 0.0950]	0.0833	[-0.1948, 0.2452]	0.2418
1.4	1500	[-0.0416, 0.0889]	0.0752	[-0.1945, 0.2449]	0.2416
3	50	[-0.0794, 0.0886]	0.0838	[-0.1273, 0.1364]	0.1318
3	300	[-0.0492, 0.0583]	0.0535	[-0.1226, 0.1317]	0.1270
3	500	[-0.0428, 0.0520]	0.0472	[-0.1222, 0.1313]	0.1266
3	1000	[-0.0353, 0.0445]	0.0396	[-0.1219, 0.1310]	0.1263
3	1500	[-0.0315, 0.0407]	0.0358	[-0.1218, 0.1309]	0.1262
3	2000	[-0.0258, 0.0350]	0.0301	[-0.1217, 0.1308]	0.1261

TABLE II: Bounds on the \hat{a}_V magnetic moment and \hat{a}_A electric dipole moment for the process $\gamma e^- \rightarrow \bar{t} b \nu_e$ (γ is the Compton backscattering photon) for b – tagging efficiency = 0.8, $\delta_{sys} = 0\%$, 5% at 2σ and 3σ C.L.

2 σ C.L.		$\delta_{sys} = 0\%$		$\delta_{sys} = 5\%$	
\sqrt{s} (TeV)	\mathcal{L} (fb^{-1})	\hat{a}_V	$ \hat{a}_A $	\hat{a}_V	$ \hat{a}_A $
1.4	50	[-0.1624, 0.2158]	0.1872	[-0.2198, 0.2733]	0.2451
1.4	300	[-0.0958, 0.1493]	0.1196	[-0.2003, 0.2538]	0.2255
1.4	500	[-0.0882, 0.1353]	0.1052	[-0.1985, 0.2520]	0.2237
1.4	1000	[-0.0657, 0.1192]	0.0885	[-0.1971, 0.2506]	0.2223
1.4	1500	[-0.0576, 0.1111]	0.0800	[-0.1967, 0.2501]	0.2218
3	50	[-0.0845, 0.0936]	0.0887	[-0.1201, 0.1292]	0.1246
3	300	[-0.0523, 0.0614]	0.0563	[-0.1127, 0.1218]	0.1172
3	500	[-0.0454, 0.0545]	0.0494	[-0.1120, 0.1212]	0.1165
3	1000	[-0.0375, 0.0465]	0.0414	[-0.1115, 0.1207]	0.1160
3	1500	[-0.0334, 0.0425]	0.0373	[-0.1114, 0.1205]	0.1159
3	2000	[-0.0273, 0.0364]	0.0312	[-0.1113, 0.1204]	0.1158
3 σ C.L.		$\delta_{sys} = 0\%$		$\delta_{sys} = 5\%$	
1.4	50	[-0.1793, 0.2327]	0.2043	[-0.2420, 0.2955]	0.2674
1.4	300	[-0.1065, 0.1599]	0.1305	[-0.2207, 0.2742]	0.2460
1.4	500	[-0.0912, 0.1447]	0.1149	[-0.2188, 0.2722]	0.2440
1.4	1000	[-0.0735, 0.1269]	0.0969	[-0.2172, 0.2707]	0.2425
1.4	1500	[-0.0645, 0.1180]	0.0873	[-0.2167, 0.2702]	0.2420
3	50	[-0.0926, 0.1017]	0.0966	[-0.1315, 0.1406]	0.1360
3	300	[-0.0574, 0.0665]	0.0616	[-0.1234, 0.1325]	0.1279
3	500	[-0.0500, 0.0591]	0.0541	[-0.1226, 0.1318]	0.1271
3	1000	[-0.0413, 0.0504]	0.0453	[-0.1221, 0.1312]	0.1266
3	1500	[-0.0368, 0.0459]	0.0408	[-0.1219, 0.1310]	0.1264
3	2000	[-0.0301, 0.0392]	0.0341	[-0.1218, 0.1309]	0.1263

shows improvement by a factor of 1.8 with respect to the unpolarized case.

TABLE III: Total cross sections for the process $\gamma e^- \rightarrow \bar{t} b \nu_e$ (γ is the Compton backscattering photon) as a function of \hat{a}_V and \hat{a}_A for b -tagging efficiency = 0.8 at $P_{e^-,e^+} = -80\%, 0\%$ and $P_{e^-,e^+} = 0\%, 0\%$, respectively.

$P_{e^-,e^+} = -80\%, 0\%$				
$\sqrt{s} (TeV)$	\hat{a}_V	$\sigma_{Tot}(\gamma e^- \rightarrow \bar{t} b \nu_e)(pb)$	\hat{a}_A	$\sigma_{Tot}(\gamma e^- \rightarrow \bar{t} b \nu_e)(pb)$
1.4	-1	1.4328×10^{-1}	-1	1.3862×10^{-1}
1.4	-0.5	7.5675×10^{-2}	-0.5	7.3354×10^{-2}
1.4	0	5.1582×10^{-2} (SM)	0	5.1582×10^{-2} (SM)
1.4	0.5	7.1010×10^{-2}	0.5	7.3332×10^{-2}
1.4	1	1.3393×10^{-1}	1	1.3862×10^{-1}
3	-1	5.4330×10^{-1}	-1	5.3912×10^{-1}
3	-0.5	1.9331×10^{-1}	-0.5	1.9120×10^{-1}
3	0	7.5185×10^{-2} (SM)	0	7.5185×10^{-2} (SM)
3	0.5	1.8907×10^{-1}	0.5	1.9117×10^{-1}
3	1	5.3492×10^{-1}	1	5.3923×10^{-1}
$P_{e^-,e^+} = 0\%, 0\%$				
1.4	-1	7.9603×10^{-2}	-1	7.7002×10^{-2}
1.4	-0.5	4.2039×10^{-2}	-0.5	4.0744×10^{-2}
1.4	0	2.8659×10^{-2} (SM)	0	2.8659×10^{-2} (SM)
1.4	0.5	3.9456×10^{-2}	0.5	4.0742×10^{-2}
1.4	1	7.4405×10^{-2}	1	7.7019×10^{-2}
3	-1	3.0186×10^{-1}	-1	2.9953×10^{-1}
3	-0.5	1.0738×10^{-1}	-0.5	1.0621×10^{-1}
3	0	4.1765×10^{-2} (SM)	0	4.1765×10^{-2} (SM)
3	0.5	1.0502×10^{-1}	0.5	1.0620×10^{-1}
3	1	2.9713×10^{-1}	1	2.9952×10^{-1}

III. WEIZSACKER-WILLIAMS APPROXIMATION (WWA): CROSS SECTION OF $e^+e^- \rightarrow e^+\gamma^*e^- \rightarrow \bar{t}b\nu_e e^+$

We use the WWA and consider the process $e^+e^- \rightarrow e^+\gamma^*e^- \rightarrow \bar{t}b\nu_e e^+$ which is potentially useful for studying the dipole moments of the top quark with polarized and unpolarized e^- beams and for the center-of-mass energies of the CLIC [14].

A. Top quark dipole moments through the process $e^+e^- \rightarrow e^+\gamma^*e^- \rightarrow \bar{t}b\nu_e e^+$ with polarized and unpolarized beams

The Feynman diagrams for the subprocess $\gamma^*e^- \rightarrow \bar{t}b\nu_e$ are shown in Fig. 2. The total cross section of the subprocess depends on the contribution of the SM, (diagrams (1)-(3)) plus the contribution of the anomalous couplings (diagram (4)).

For the study of the process $e^+e^- \rightarrow e^+\gamma^*e^- \rightarrow \bar{t}b\nu_e e^+$, in Fig. 5 we show the total cross section as a function of the electromagnetic form factors of the top quark \hat{a}_V and \hat{a}_A for $P_{e^-,e^+} = -80\%, 0\%$ [61], two different center-of-mass energies $\sqrt{s} = 1.4, 3 TeV$ [14] and the Weizsacker-Williams photon virtuality $Q^2 = 2 GeV^2$ [65–68]. We can see from this figure that the total cross section changes strongly with \sqrt{s} reaching 20% and 23% at the end of the range considered to $\hat{a}_{V,A}$ with polarized and unpolarized beams.

In Fig. 6 we present the limit contours for the dipole moments in the $(\hat{a}_V - \hat{a}_A)$ plane for the process $e^+e^- \rightarrow e^+\gamma^*e^- \rightarrow \bar{t}b\nu_e e^+$. The curves are for $\sqrt{s} = 1.4, 3 TeV$ and $\mathcal{L} = 50, 500, 1500 fb^{-1}$. We have used $Q^2 = 2 GeV^2$ and b -tagging efficiency = 0.8.

We summarize the bounds obtained on the anomalous parameters \hat{a}_V and \hat{a}_A for b -tagging efficiency = 0.8, systematic uncertainties of $\delta_{sys} = 0\%, 5\%$, $\sqrt{s} = 1.4, 3 TeV$, $Q^2 = 2 GeV^2$, and $\mathcal{L} = 50, 300, 500, 1000, 1500, 2000 fb^{-1}$ at 2σ and 3σ in Tables IV and V. The bounds obtained on these parameters with polarized/unpolarized beams are slightly moderate with respect to those obtained by the process $\gamma e^- \rightarrow \bar{t}b\nu_e$ as shown in Tables I (II) and IV (V), respectively.

Finally, the predicted values of the corresponding production total cross sections of the process $e^+e^- \rightarrow e^+\gamma^*e^- \rightarrow \bar{t}b\nu_e e^+$ are listed in Table VI as a function of \hat{a}_V and \hat{a}_A by assuming the initial electron (positron) beam polarization to be -80% (0%) for $Q^2 = 2 GeV^2$, b -tagging efficiency=0.8 and center-of-mass energies of $CLIC - 1.4 TeV$ and $CLIC - 3 TeV$.

TABLE IV: Bounds on the \hat{a}_V magnetic moment and \hat{a}_A electric dipole moment for the process $e^+e^- \rightarrow e^+\gamma^*e^- \rightarrow \bar{t}b\nu_e e^+$ (γ^* is the Weizsacker-Williams photon) for $Q^2 = 2 \text{ GeV}^2$, $P_{e^-,e^+} = -80\%, 0\%$, b -tagging efficiency = 0.8, $\delta_{sys} = 0\%, 5\%$ at 2σ and 3σ C.L.

2 σ C.L.		$\delta_{sys} = 0\%$		$\delta_{sys} = 5\%$	
$\sqrt{s} \text{ (TeV)}$	$\mathcal{L} \text{ (fb}^{-1}\text{)}$	\hat{a}_V	$ \hat{a}_A $	\hat{a}_V	$ \hat{a}_A $
1.4	50	[-0.3474, 0.4397]	0.3908	[-0.3669, 0.4592]	0.4104
1.4	300	[-0.2078, 0.3001]	0.2497	[-0.2647, 0.3570]	0.3074
1.4	500	[-0.1784, 0.2707]	0.2197	[-0.2505, 0.3428]	0.2931
1.4	1000	[-0.1443, 0.2366]	0.1848	[-0.2383, 0.3306]	0.2807
1.4	1500	[-0.1271, 0.2194]	0.1670	[-0.2339, 0.3262]	0.2762
3	50	[-0.1806, 0.2180]	0.1984	[-0.2037, 0.2411]	0.2216
3	300	[-0.1094, 0.1469]	0.1267	[-0.1652, 0.2026]	0.1829
3	500	[-0.0944, 0.1318]	0.1115	[-0.1608, 0.1982]	0.1785
3	1000	[-0.0769, 0.1144]	0.0937	[-0.1573, 0.1947]	0.1750
3	1500	[-0.0681, 0.1055]	0.0847	[-0.1561, 0.1935]	0.1738
3	2000	[-0.0547, 0.0921]	0.0713	[-0.1555, 0.1929]	0.1732
3 σ C.L.		$\delta_{sys} = 0\%$		$\delta_{sys} = 5\%$	
1.4	50	[-0.3827, 0.4750]	0.4264	[-0.4040, 0.4963]	0.4478
1.4	300	[-0.2302, 0.3225]	0.2724	[-0.2924, 0.3847]	0.3354
1.4	500	[-0.1980, 0.2903]	0.2397	[-0.2769, 0.3692]	0.3197
1.4	1000	[-0.1607, 0.2530]	0.2016	[-0.2636, 0.3559]	0.3063
1.4	1500	[-0.1418, 0.2341]	0.1822	[-0.2587, 0.3510]	0.3013
3	50	[-0.1986, 0.2360]	0.2165	[-0.2238, 0.2612]	0.2418
3	300	[-0.1208, 0.1583]	0.1383	[-0.1817, 0.2191]	0.1995
3	500	[-0.1044, 0.1419]	0.1217	[-0.1770, 0.2144]	0.1948
3	1000	[-0.0853, 0.1228]	0.1023	[-0.1732, 0.2106]	0.1909
3	1500	[-0.0756, 0.1131]	0.0924	[-0.1718, 0.2092]	0.1896
3	2000	[-0.0609, 0.1081]	0.0777	[-0.1711, 0.2086]	0.1890

TABLE V: Bounds on the \hat{a}_V magnetic moment and \hat{a}_A electric dipole moment for the process $e^+e^- \rightarrow e^+\gamma^*e^- \rightarrow \bar{t}b\nu_e e^+$ (γ^* is the Weizsacker-Williams photon) for $Q^2 = 2 GeV^2$, b -tagging efficiency = 0.8, $\delta_{sys} = 0\%$, 5% at 2σ and 3σ C.L.

2 σ C.L.		$\delta_{sys} = 0\%$		$\delta_{sys} = 5\%$	
\sqrt{s} (TeV)	\mathcal{L} (fb^{-1})	\hat{a}_V	$ \hat{a}_A $	\hat{a}_V	$ \hat{a}_A $
1.4	50	[-0.4088, 0.5012]	0.4527	[-0.4219, 0.5142]	0.4657
1.4	300	[-0.2467, 0.3390]	0.2892	[-0.2883, 0.3806]	0.3313
1.4	500	[-0.2126, 0.0304]	0.2545	[-0.2673, 0.3597]	0.3101
1.4	1000	[-0.1728, 0.2651]	0.2140	[-0.2482, 0.3405]	0.2907
1.4	1500	[-0.1527, 0.2450]	0.1934	[-0.2409, 0.3332]	0.2833
3	50	[-0.2126, 0.2493]	0.2299	[-0.2274, 0.2654]	0.2459
3	300	[-0.1300, 0.1666]	0.1468	[-0.1726, 0.2106]	0.1908
3	500	[-0.1125, 0.1491]	0.1293	[-0.1656, 0.2035]	0.1838
3	1000	[-0.0921, 0.1287]	0.1086	[-0.1597, 0.1977]	0.1778
3	1500	[-0.0818, 0.1184]	0.0982	[-0.1576, 0.1956]	0.1757
3	2000	[-0.0662, 0.1028]	0.0826	[-0.1565, 0.1945]	0.1747
3 σ C.L.		$\delta_{sys} = 0\%$		$\delta_{sys} = 5\%$	
1.4	50	[-0.4499, 0.5422]	0.4938	[-0.4641, 0.5554]	0.5081
1.4	300	[-0.2727, 0.3651]	0.3155	[-0.3182, 0.4105]	0.3614
1.4	500	[-0.2354, 0.3277]	0.2777	[-0.2953, 0.3876]	0.3383
1.4	1000	[-0.1919, 0.2842]	0.2335	[-0.2744, 0.3667]	0.3171
1.4	1500	[-0.1698, 0.2622]	0.2111	[-0.2664, 0.3587]	0.3091
3	50	[-0.2335, 0.2702]	0.2508	[-0.2497, 0.2877]	0.2682
3	300	[-0.1433, 0.1799]	0.1602	[-0.1899, 0.2279]	0.2082
3	500	[-0.1242, 0.1607]	0.1410	[-0.1822, 0.2202]	0.2005
3	1000	[-0.1019, 0.1385]	0.1185	[-0.1758, 0.2138]	0.1940
3	1500	[-0.0906, 0.1272]	0.1071	[-0.1735, 0.2115]	0.1917
3	2000	[-0.0736, 0.1102]	0.0901	[-0.1723, 0.2103]	0.1906

It is worth mentioning that the ratio of the total cross section of the process $\gamma e^- \rightarrow \bar{t} b \nu_e$ (γ is the Compton backscattering photon) is generally about 18 times greater than the total cross section of the process $e^+ e^- \rightarrow e^+ \gamma^* e^- \rightarrow \bar{t} b \nu_e e^+$ (γ^* is the Weizsacker-Williams photon) and both total cross sections depend strongly on the dipole moments (\hat{a}_V and \hat{a}_A) and on the center-of-mass energy (\sqrt{s}) of the CLIC.

IV. CONCLUSIONS

Although γe^- and $\gamma\gamma$ processes require new detectors, $\gamma^* e^-$ and $\gamma^* \gamma^*$ are produced spontaneously at linear colliders without any detectors. These processes will allow the future linear colliders to operate in two different modes, $\gamma^* e^-$ and $\gamma^* \gamma^*$, opening up the opportunity for a wider search for new physics. Therefore, the $\gamma^* e^-$ linear collisions represent an excellent opportunity to study top quark anomalous magnetic moment and electric dipole moment.

We have performed a study of the total cross section of the processes $\gamma e^- \rightarrow \bar{t} b \nu_e$ and $e^+ e^- \rightarrow e^+ \gamma^* e^- \rightarrow \bar{t} b \nu_e e^+$, with polarized and unpolarized electron beams as a function of the anomalous couplings \hat{a}_V and \hat{a}_A . We have also investigated anomalous \hat{a}_V and \hat{a}_A couplings for both polarized and unpolarized cases. The general behavior of the cross sections as a function of \hat{a}_V and \hat{a}_A couplings does not change. However, we can see from our calculations of the polarized and unpolarized cases that polarization increases the cross sections. The main reason for these results can be seen in Fig. 2. There are four diagrams which contribute to the process and one of them includes the $t\bar{t}\gamma$ vertex. This diagram gives the maximum contribution to the total cross section. For $P_{e^-,e^+} = -80\%, 0\%$, this contribution is dominant due to the structure of the $W e^- \nu_e$ vertex. We can appreciate from these figures that lepton polarization can improve the bounds on the anomalous couplings. The analysis is shown in Figs. 3 and 5 with Compton backscattering photon and Weizsacker-Williams photon virtuality of $Q^2 = 2 \text{ GeV}^2$ and b -tagging efficiency = 0.8. In both processes, the cross section shows a strong dependence on the anomalous couplings \hat{a}_V and \hat{a}_A , as well as on the center-of-mass energy \sqrt{s} . This variation of the cross section for $\sqrt{s} = 1.4, 3 \text{ TeV}$ is of the order 24.5%, 26.6% and 20%, 23% for $\gamma e^- \rightarrow \bar{t} b \nu_e$ and $e^+ e^- \rightarrow e^+ \gamma^* e^- \rightarrow \bar{t} b \nu_e e^+$, respectively.

We also include contour plots for the dipole moments at the 95% *C.L.* in the $(\hat{a}_V - \hat{a}_A)$

TABLE VI: Total cross sections for the process $e^+e^- \rightarrow e^+\gamma^*e^- \rightarrow \bar{t}b\nu_e e^+$ (γ^* is the Weizsacker-Williams photon) as a function of \hat{a}_V and \hat{a}_A for $Q^2 = 2 \text{ GeV}^2$, b - tagging efficiency = 0.8 at $P_{e^-,e^+} = -80\%, 0\%$ and $P_{e^-,e^+} = 0\%, 0\%$, respectively.

$P_{e^-,e^+} = -80\%, 0\%$				
$\sqrt{s}(\text{TeV})$	\hat{a}_V	$\sigma_{Tot}(e^+e^- \rightarrow e^+\gamma^*e^- \rightarrow \bar{t}b\nu_e e^+)(\text{pb})$	\hat{a}_A	$\sigma_{Tot}(e^+e^- \rightarrow e^+\gamma^*e^- \rightarrow \bar{t}b\nu_e e^+)(\text{pb})$
1.4	-1	7.2429×10^{-3}	-1	6.9011×10^{-3}
1.4	-0.5	4.2934×10^{-3}	-0.5	4.1221×10^{-3}
1.4	0	3.1962×10^{-3} (SM)	0	3.1962×10^{-3} (SM)
1.4	0.5	3.9510×10^{-3}	0.5	4.1219×10^{-3}
1.4	1	6.5593×10^{-3}	1	6.9011×10^{-3}
3	-1	3.2064×10^{-2}	-1	3.1205×10^{-2}
3	-0.5	1.4380×10^{-2}	-0.5	1.3952×10^{-2}
3	0	8.1986×10^{-3} (SM)	0	8.1986×10^{-3} (SM)
3	0.5	1.3521×10^{-2}	0.5	1.3951×10^{-2}
3	1	3.0346×10^{-2}	1	3.1208×10^{-2}
$P_{e^-,e^+} = 0\%, 0\%$				
1.4	-1	4.0240×10^{-3}	-1	3.8340×10^{-3}
1.4	-0.5	2.3853×10^{-3}	-0.5	2.2903×10^{-3}
1.4	0	1.7754×10^{-3} (SM)	0	1.7754×10^{-3} (SM)
1.4	0.5	2.1950×10^{-3}	0.5	2.2901×10^{-3}
1.4	1	3.6438×10^{-3}	1	3.8338×10^{-3}
3	-1	1.7875×10^{-2}	-1	1.7336×10^{-2}
3	-0.5	7.9900×10^{-3}	-0.5	7.7515×10^{-3}
3	0	4.5559×10^{-3} (SM)	0	4.5559×10^{-3} (SM)
3	0.5	7.5127×10^{-3}	0.5	7.7508×10^{-3}
3	1	1.6860×10^{-2}	1	1.7337×10^{-2}

plane for the processes $\gamma e^- \rightarrow \bar{t}b\nu_e$ and $e^+e^- \rightarrow e^+\gamma^*e^- \rightarrow \bar{t}b\nu_e e^+$ for $Q^2 = 2 \text{ GeV}^2$ and

$\sqrt{s} = 1.4, 3 \text{ TeV}$ in Figs. 4 and 6. The contours are consistent with the results obtained in Tables I, II, IV and V. The bounds obtained in these Tables are competitive with those recently reported in the literature [51–54] and we can observe a strong correlation between the center-of-mass energy \sqrt{s} , integrated luminosity \mathcal{L} and the dipole moments \hat{a}_V and \hat{a}_A .

Other promising production modes for studying the cross section and the electromagnetic dipole moments \hat{a}_V and \hat{a}_A of the top quark are the processes $\gamma\gamma \rightarrow t\bar{t}$ (Compton backscattering photon), $\gamma^*\gamma^* \rightarrow t\bar{t}$ (Weizsacker-Williams photon) and $\gamma\gamma^* \rightarrow t\bar{t}$ (Compton backscattering photon, Weizsacker-Williams photon), respectively. These processes are one of the most important sources of $t\bar{t}$ pair production and represent new physics effects at a high-energy and high-luminosity linear electron positron collider as the CLIC.

In conclusion, we have found that the processes $\gamma e^- \rightarrow \bar{t}b\nu_e$ and $e^+e^- \rightarrow e^+\gamma^*e^- \rightarrow \bar{t}b\nu_e e^+$ in the γe^- and γ^*e^- collision modes at the high energies and luminosities expected at the CLIC can be used as a probe to bound the magnetic moment \hat{a}_V and electric dipole moment \hat{a}_A of the top quark. In particular, using integrated luminosity 2 ab^{-1} , center-of-mass energies of 3 TeV , b – tagging efficiency = 0.8 and considering the systematic uncertainty $\delta_{sys} = 5\%$, we derive bounds on the dipole moments of the top quark at 2σ and 3σ (90% and 95%) C.L.: $-0.1112 (-0.1217) \leq \hat{a}_V \leq 0.1203 (0.1308)$, $|\hat{a}_A| = 0.1156 (0.1261)$ and $-0.1113 (-0.1218) \leq \hat{a}_V \leq 0.1204 (0.1309)$, $|\hat{a}_A| = 0.1158 (0.1263)$ for $\gamma e^- \rightarrow \bar{t}b\nu_e$ with unpolarized and polarized e^- beams. For $e^+e^- \rightarrow e^+\gamma^*e^- \rightarrow \bar{t}b\nu_e e^+$ with polarized and unpolarized electron beams, $-0.1555 (-0.1711) \leq \hat{a}_V \leq 0.1929 (0.2086)$, $|\hat{a}_A| = 0.1732 (0.1890)$ and $-0.1565 (-0.1723) \leq \hat{a}_V \leq 0.1945 (0.2103)$, $|\hat{a}_A| = 0.1747 (0.1906)$. These results are competitive with those recently reported in previous studies [51–54]. To our knowledge, our numerical results for the dipole moments of the top quark through the single top production processes have never been reported in the literature before and could be of relevance for the scientific community.

Acknowledgments

A. G. R. acknowledges support from CONACyT, SNI and PROFOCIE (México).

-
- [1] S. L. Glashow, *Nucl. Phys.* **22**, 579 (1961).
- [2] S. Weinberg, *Phys. Rev. Lett.* **19**, 1264 (1967).
- [3] A. Salam, in *Elementary Particle Theory*, Ed. N. Svartholm (Almquist and Wiksell, Stockholm, 1968) 367.
- [4] K. A. Olive, *et al.*, [Particle Data Group], *Chin. Phys.* **C38**, 090001 (2014).
- [5] ATLAS Collaboration, *Measurement of the inclusive $t\bar{t}\gamma$ cross section with the ATLAS detector*, Tech. Rep. ATLAS-CONF-2011-153, ATLAS-COM-CONF-2011-186, 2011.
- [6] CMS Collaboration, *Measurement of the inclusive top-quark pair + photon production cross section in the muon + jets channel in pp collisions at 8 TeV*, Tech. Rep. CMS-PAS-TOP-13-011, 2014.
- [7] T. Abe, *et al.* [Am. LC Group], arXiv:hep-ex/0106055, arXiv:hep-ex/0106056, arXiv:hep-ex/0106057, arXiv:hep-ex/0106058, and references therein.
- [8] G. Aarons, *et al.*, [ILC Collaboration], arXiv:0709.1893 [hep-ph].
- [9] J. Brau, *et al.*, [ILC Collaboration], arXiv:0712.1950 [physics.acc-ph].
- [10] H. Baer, T. Barklow, K. Fujii, *et al.*, arXiv:1306.6352 [hep-ph].
- [11] E. Accomando, *et al.*, [CLIC Phys. Working Group Collaboration], arXiv:hep-ph/0412251, CERN-2004-005.
- [12] D. Dannheim, P. Lebrun, L. Linssen, *et al.*, arXiv:1208.1402 [hep-ex].
- [13] J. A. Aguilar-Saavedra, *et al.*, [TESLA: The Superconducting electron positron linear collider with an integrated x-ray laser laboratory. Technical design report. Part 3. Physics at an e^+e^- linear collider], arXiv:hep-ph/0106315, and references therein.
- [14] H. Abramowicz, *et al.*, [The CLIC Detector and Physics Study], arXiv:1307.5288 [hep-ex].
- [15] A. Soni and R. M. Xu, *Phys. Rev. Lett.* **69**, 33 (1992).
- [16] A. Soni and R. M. Xu, *Phys. Rev.* **D45**, 2405 (1992).
- [17] A. Bartl, E. Christova, T. Gajdosik and W. Majerotto, *Nucl. Phys. Proc. Suppl.* **66**, 75 (1998).
- [18] W. Hollik, J. I. Illana, S. Rigolin, C. Schappacher and D. Stockinger, *Nucl. Phys.* **551B**, 3 (1999) [Erratum-ibid. **B557**, 407 (1999)].
- [19] C. S. Huang and T. J. Li, *Z. Phys.* **68C**, 319 (1995).
- [20] G. A. González-Sprinberg, R. Martínez and J. Vidal, *JHEP* **1107**, 094 (2011).

- [21] R. Martínez and J. Alexis Rodríguez, *Phys. Rev.* **D60**, 077504 (1999).
- [22] F. Larios, M. A. Pérez and C. P. Yuan, *Phys. Lett.* **B457**, 334 (1999).
- [23] D. Atwood, A. Aeppli and A. Soni, *Phys. Rev. Lett.* **69**, 2754 (1992).
- [24] P. Poulouze and S. D. Rindani, *Phys. Rev.* **D57**, 5444 (1998) [Erratum-ibid. **D61** , 119902 (2000)].
- [25] S. Y. Choi and K. Hagiwara, *Phys. Lett.* **B359**, 369 (1995).
- [26] P. Poulouze and S. D. Rindani, *Phys. Rev.* **D91**, 093008 (2015).
- [27] E. Boos, M. Dubinin, A. Pukhov, M. Sachwitz and H. J. Schreiber, *Eur. Phys. J.* **C21**, 81 (2001) and references therein.
- [28] Puneet Batra and Timothy M. P. Tait, *Phys. Rev.* **D74**, 054021 (2006).
- [29] J. Fuster, *et al.*, *Eur. Phys. J.* **C75**, 223 (2015) and references therein.
- [30] E. Boos and L. Dudko, *Int. J. Mod. Phys.* **A27**, 1230026 (2012) and references therein.
- [31] E. Boos, *Nucl. Instrum. Meth.* **A472**, 22 (2001) and references therein.
- [32] E. Boos, A. Pukhov, M. Sachwitz, H. J. Schreiber, *Phys. Lett.* **B404**, 119 (1997).
- [33] G. Jikia, *Nucl. Phys.* **B374**, 83 (1992).
- [34] E. Boos, *et al.*, *Z. Phys.* **C70**, 255 (1996).
- [35] E. Boos, *et al.*, *Z. Phys.* **C75**, 237 (1997).
- [36] Jun-Jie Cao, *et al.*, *Phys. Rev.* **D58**, 094004 (1998).
- [37] G. Weiglein, *et al.* [LHC/LC Study Group Collaboration], *Phys. Rept.* **426**, 47 (2006).
- [38] A. P. Heinson, A.S. Belyaev and E. E. Boos, *Phys. Rev.* **D56**, 3114 (1997).
- [39] D. O. Carlson and C.P. Yuan, *Phys. Lett.* **B306**, 386 (1993).
- [40] D. O. Carlson, E. Malkawi and C. P. Yuan, *Phys. Lett.* **B337**, 145 (1994).
- [41] E. H. Simmons, *Phys. Rev.* **D55**, 5494 (1997).
- [42] D. Atwood, S. Bar-Shalom, G. Eilam and A. Soni, *Phys. Rev.* **D54**, 5412 (1996).
- [43] C. S. Li, R. J. Oakes and J. M. Yang, *Phys. Rev.* **D55**, 1672 (1997).
- [44] E. Malkawi and T. Tait, *Phys. Rev.* **D54**, 5758 (1996).
- [45] A. Datta, J. M. Yang, B. Young and X. Zhang, *Phys. Rev.* **D56**, 3107 (1997).
- [46] R. J. Oakes, K. Whisnant, J. M. Yang, B. Young and X. Zhang, *Phys. Rev.* **D57**, 534 (1998).
- [47] W. Bernreuther, *et al.*, *Phys. Rev. Lett.* **95**, 261802 (2005) and references therein.
- [48] M. E. Pospelov and I. B. Khriplovich, *Sov. J. Nucl. Phys.* **53**, 638 (1991) [*Yad. Fiz.* 53 (1991) 1030].

- [49] F. Hoogeveen, *Nucl. Phys.* **B341**, 322 (1990).
- [50] T. Ibrahim and P. Nath, *Phys. Rev.* **D82**, 055001 (2010).
- [51] U. Baur, A. Juste, L. H. Orr and D. Rainwater, *Phys. Rev.* **D71**, 054013 (2005).
- [52] A. O. Bouzas and F. Larios, *Phys. Rev.* **D87**, 074015 (2013).
- [53] A. O. Bouzas and F. Larios, *Phys. Rev.* **D88**, 094007 (2013).
- [54] Sh. Fayazbakhsh, S. Taheri Monfared and M. Mohammadi Najafabadi, *Phys. Rev.* **D92**, 014006 (2015).
- [55] M. S. Amjad, *et al.*, arXiv:1307.8102 [hep-ph], and references therein..
- [56] A. Juste, *et al.*, arXiv:hep-ph/0601112, and references therein.
- [57] D. Asner, *et al.*, arXiv:1307.8265 [hep-ex] and references therein.
- [58] J. F. Kamenik, M. Papucci and A. Weiler, *Phys. Rev.* **D85**, 071501 (2012).
- [59] J. A. Aguilar-Saavedra, *Nucl. Phys.* **B812**, 181 (2009).
- [60] J. A. Aguilar-Saavedra, M. C. N. Fiolhais and A. Onofre, *JHEP* **07**, 180 (2012).
- [61] G. Moortgat-Pick, *et al.*, *Physics Reports* **460**, 131243 (2008).
- [62] G. Baur, *et al.*, *Phys. Rep.* **364**, 359 (2002).
- [63] V. M. Budnev, I. F. Ginzburg, G. V. Meledin and V. G. Serbo, *Phys. Rep.* **15**, 181 (1975).
- [64] K. Piotrkowski, *Phys. Rev.* **D63**, 071502 (2001).
- [65] M. Acciarri, *et al.*, [L3 Collaboration], *Phys. Lett.* **B434**, 169 (1998).
- [66] K. Ackerstaff, *et al.*, [OPAL Collaboration], *Phys. Lett.* **B431**, 188 (1998).
- [67] I. Sahin, *Phys. Rev.* **D85**, 033002 (2012).
- [68] A. A. Billur, *et al.*, *Phys. Rev.* **D89**, 037301 (2014).
- [69] A. Abulencia, *et al.*, [CDF Collaboration], *Phys. Rev. Lett.* **98**, 112001 (2007).
- [70] T. Aaltonen, *et al.*, [CDF Collaboration], *Phys. Rev. Lett.* **102**, 222002 (2009).
- [71] T. Aaltonen, *et al.*, [CDF Collaboration], *Phys. Rev. Lett.* **102**, 242001 (2009).
- [72] S. Chatrchyan, *et al.*, [CMS Collaboration], *JHEP* **1201**, 052 (2012).
- [73] S. Chatrchyan, *et al.*, [CMS Collaboration], *JHEP* **1211**, 080 (2012).
- [74] V. M. Abazov, *et al.*, [D0 Collaboration], *Phys. Rev.* **D88**, 012005 (2013).
- [75] S. Chatrchyan, *et al.*, [CMS Collaboration], *JHEP* **07**, 116 (2013).
- [76] S. C. Inan, *Phys. Rev.* **D81**, 115002 (2010).
- [77] S. C. Inan, *Nucl. Phys.* **B897**, 289 (2015).
- [78] S. C. Inan, *Int. J. Mod. Phys.* **A26**, 3605 (2011).

- [79] I. Sahin and S. C. Inan, *JHEP* **0909**, 069 (2009).
- [80] S. Atag, S. C. Inan and I. Sahin, *JHEP* **1009**, 042 (2010).
- [81] I. Sahin and B. Sahin, *Phys. Rev.* **D86**, 115001 (2012).
- [82] B. Sahin and A. A. Billur, *Phys. Rev.* **D86**, 074026 (2012).
- [83] A. Senol, *Int. J. Mod. Phys.* **A29**, 1450148 (2014).
- [84] A. Senol, *Phys. Rev.* **D87**, 073003 (2013).
- [85] S. Fichet, G. von Gersdorff, B. Lenzi, C. Royon and M. Saimpert, *JHEP* **1502**, 165 (2015).
- [86] H. Sun, *Phys. Rev.* **D90**, 035018 (2014).
- [87] H. Sun, *Nucl. Phys.* **B886**, 691 (2014).
- [88] H. Sun, Y. J. Zhou and H. S. Hou, *JHEP* **1502**, 064 (2015).
- [89] A. Senol and M. Koksals, *JHEP* **1503**, 139 (2015).
- [90] S. Atag and A. A. Billur, *JHEP* **1011**, 060 (2010).
- [91] Alexander Belyaev, Neil D. Christensen and Alexander Pukhov, *Comput. Phys. Commun.* **184**, 1729 (2013), arXiv:1207.6082 [hep-ph].
- [92] G. Aad, *et al.*, [ATLAS Collaboration], *Phys. Lett.* **B717**, 330 (2012).
- [93] G. Abbiendi, *et al.*, [OPAL Collaboration], *Phys. Lett.* **B521**, 181 (2001).
- [94] M. Martinez and R. Miquel, *Eur. Phys. J.* **C27**, 49 (2003).
- [95] A. Juste, M. Martinez and D. Schulte, *Linear Collider: Physics and Detector Studies Parte E. Contributions to the Workshop, Frascati, London, Munich, Hamburg, February 1996 to November 1996.* ed. R. Settles, DESY Report 97-123E.

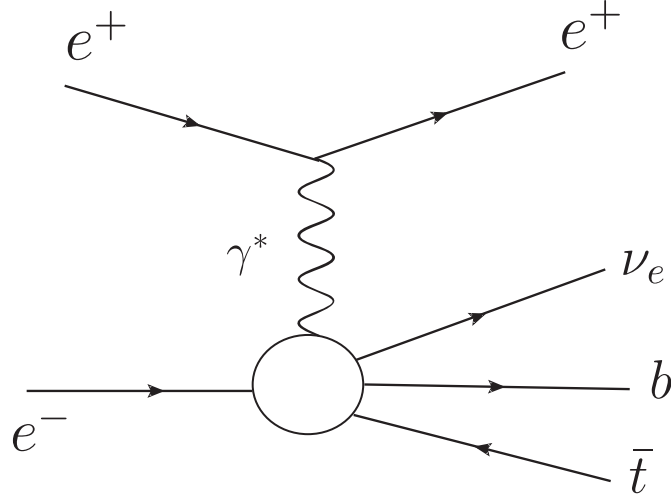


FIG. 1: Schematic diagram for the process of single top quark production $e^+e^- \rightarrow e^+\gamma^*e^- \rightarrow \bar{t}b\nu_e e^+$.

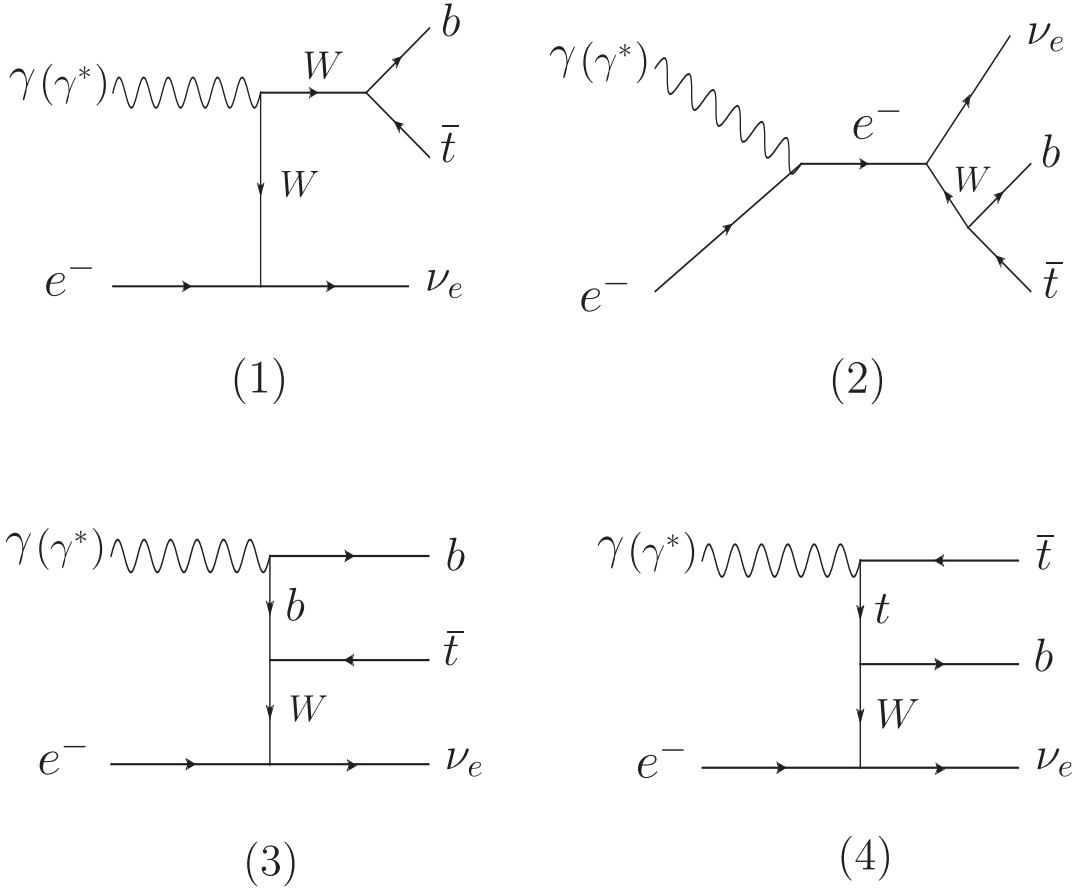


FIG. 2: The Feynman diagrams contributing to the process $\gamma e^- \rightarrow \bar{t}b\nu_e$ and the subprocess $\gamma^* e^- \rightarrow \bar{t}b\nu_e$.

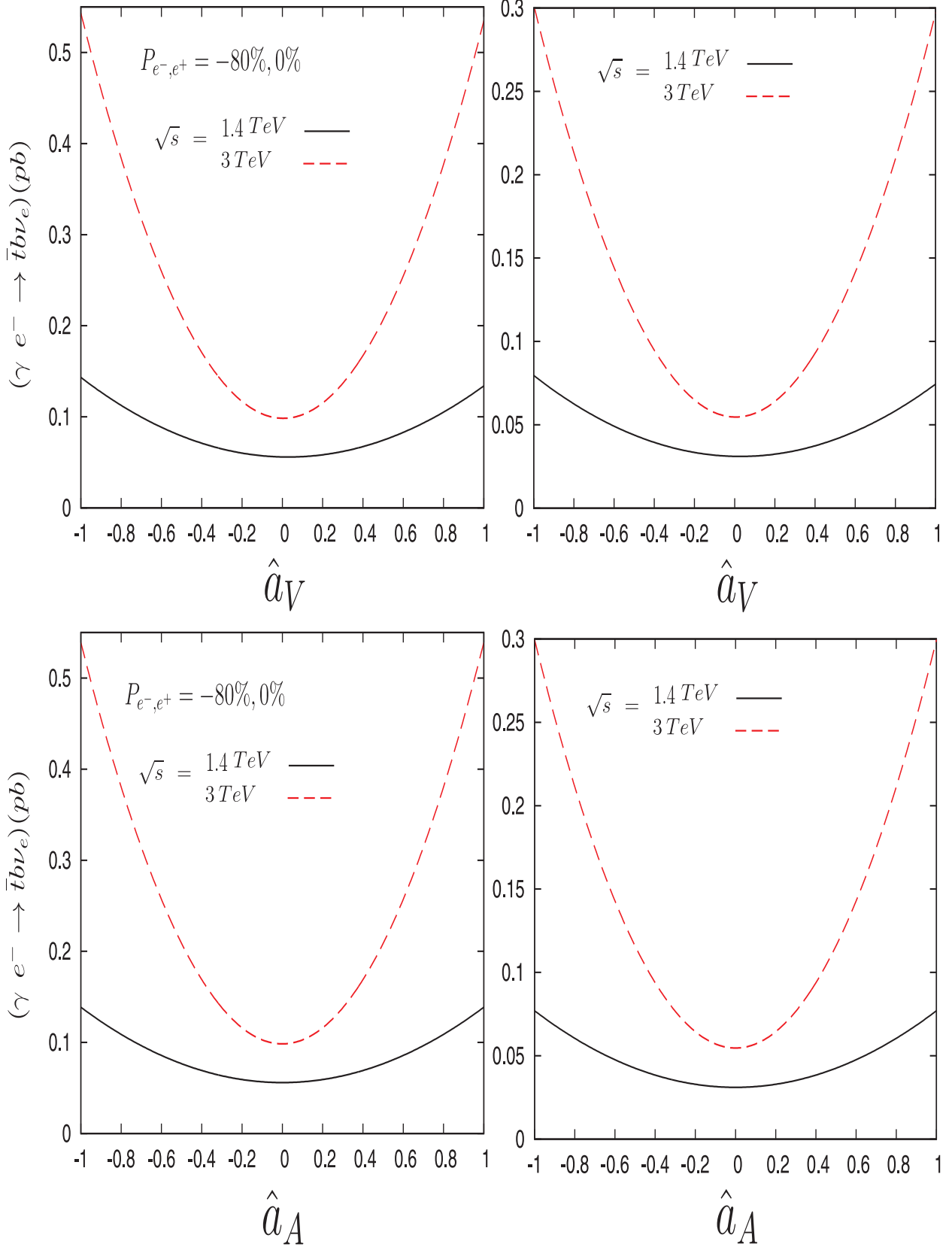


FIG. 3: The integrated total cross section of the process $\gamma e^- \rightarrow \bar{t} b \nu_e$ (γ is the Compton backscattering photon) as a function of \hat{a}_V and \hat{a}_A with $\sqrt{s} = 1.4, 3 \text{ TeV}$, and polarized and unpolarized beams.

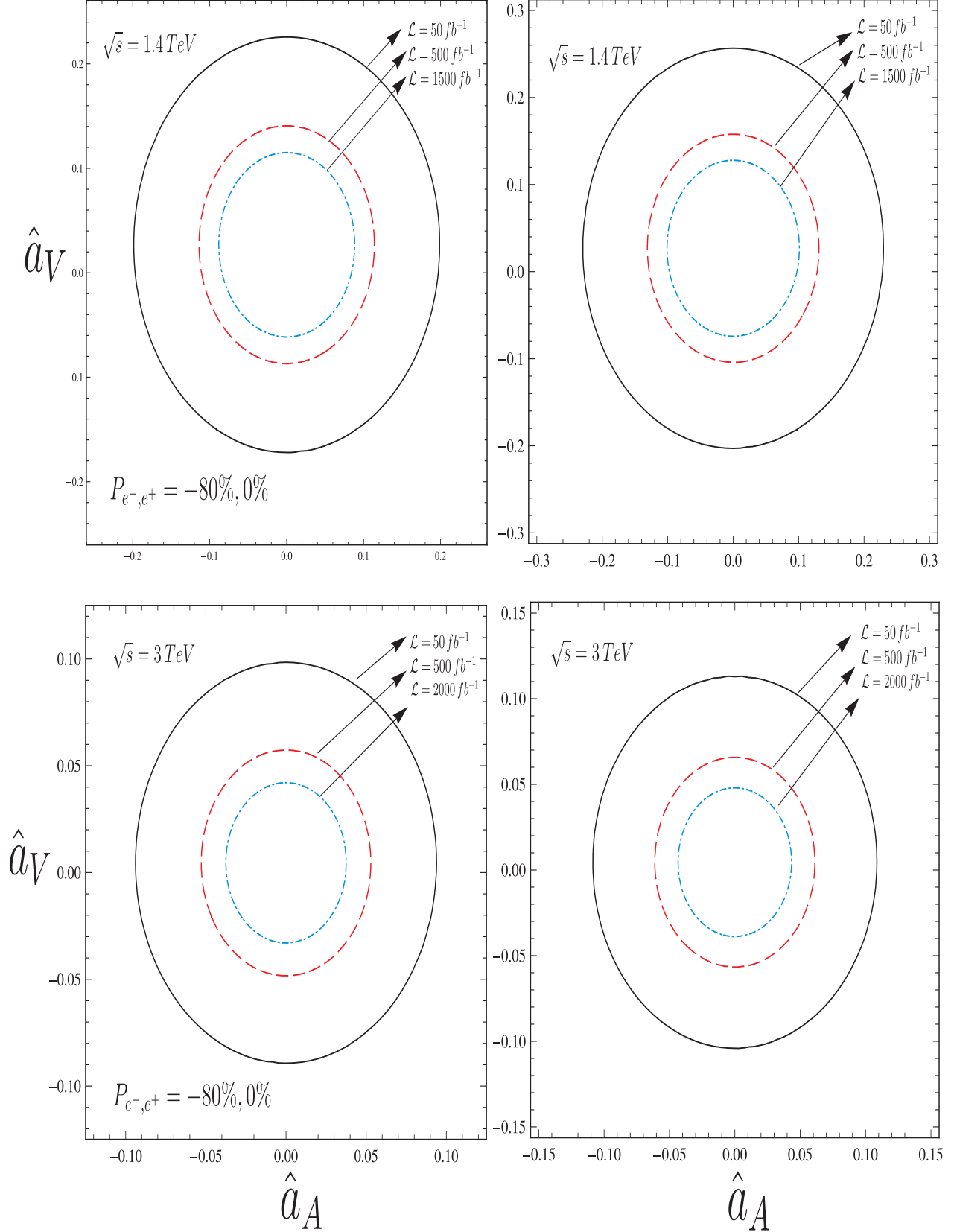


FIG. 4: Limits contours at the 95% *C.L.* in the $\hat{a}_V - \hat{a}_A$ plane for $\gamma e^- \rightarrow \bar{t} b \nu_e$ (γ is the Compton backscattering photon) and $\sqrt{s} = 1.4, 3 \text{ TeV}$ with polarized and unpolarized beams.

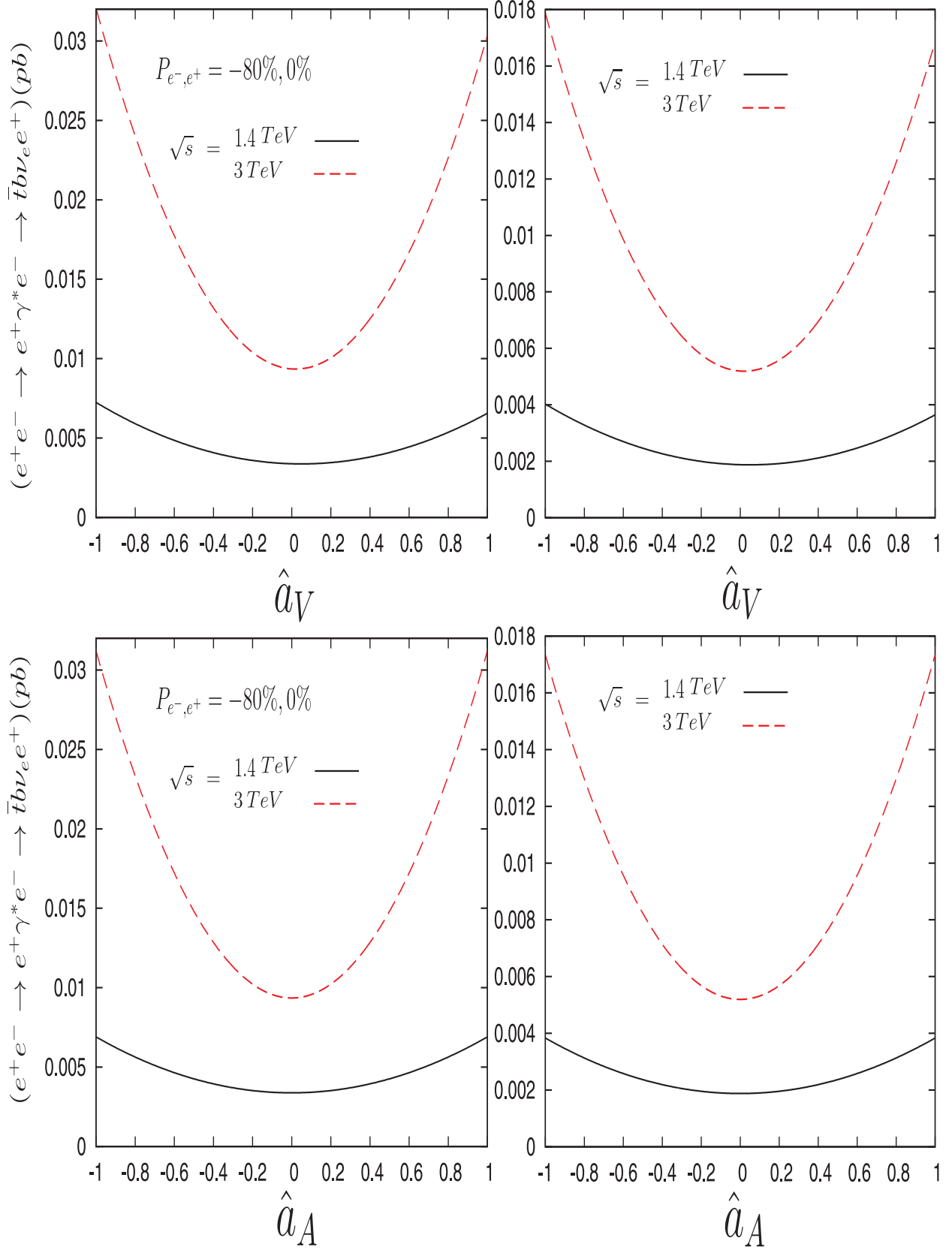


FIG. 5: The integrated total cross section of the process $e^+e^- \rightarrow e^+\gamma^*e^- \rightarrow \bar{t}b\nu_e e^+$ (γ^* is the Weizsacker-Williams photon) as a function of \hat{a}_V and \hat{a}_A with $\sqrt{s} = 1.4, 3 \text{ TeV}$, $Q^2 = 2 \text{ GeV}^2$ and polarized and unpolarized beams.

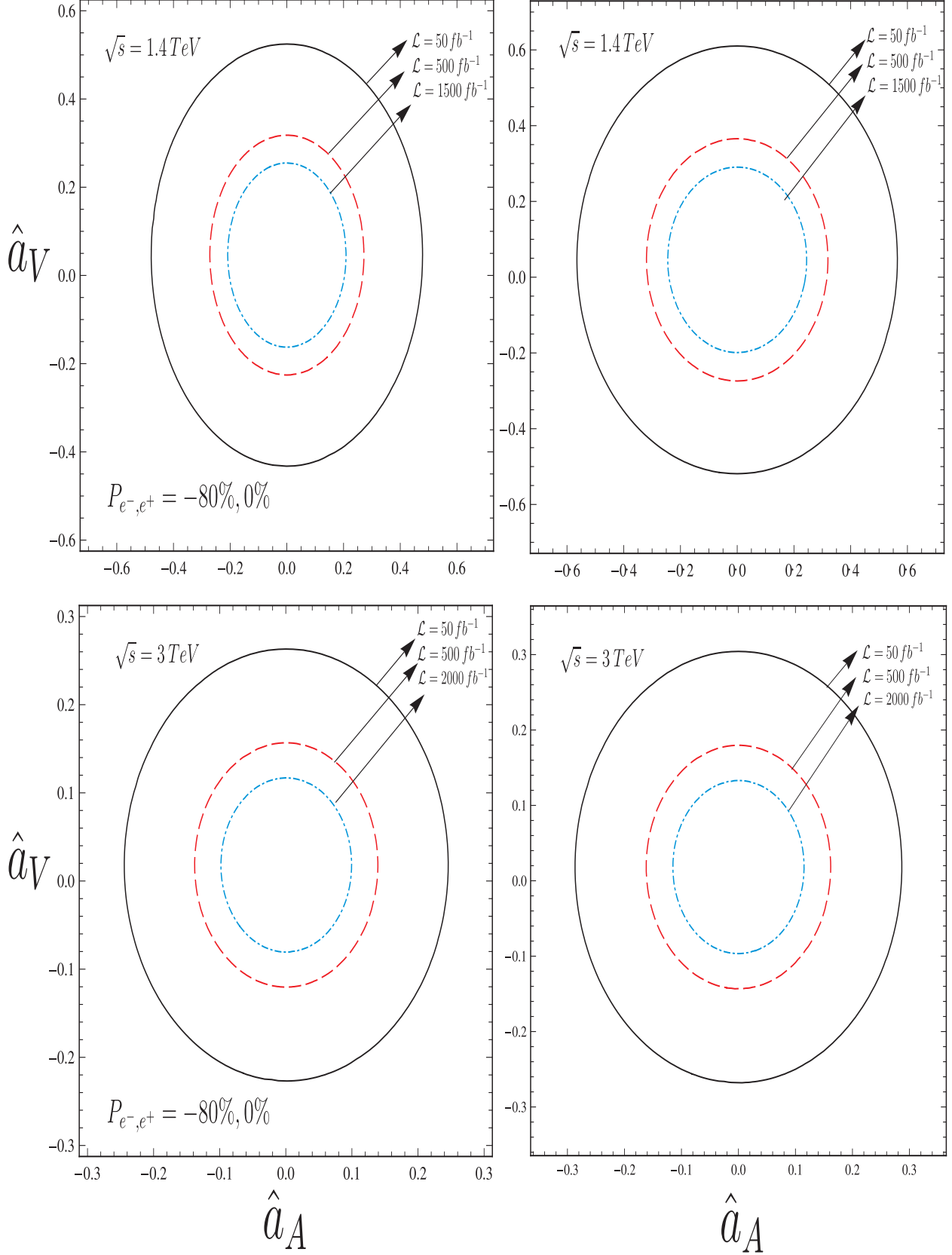


FIG. 6: Limits contours at the 95% $C.L.$ in the $\hat{a}_V - \hat{a}_A$ plane for $e^+e^- \rightarrow e^+\gamma^*e^- \rightarrow \bar{t}b\nu_e e^+$ (γ^* is the Weizsacker-Williams photon) with $\sqrt{s} = 1.4, 3 \text{ TeV}$, $Q^2 = 2 \text{ GeV}^2$ and polarized and unpolarized beams.